COBEM 2023 27TH INTERNATIONAL CONGRESS OF MECHANICAL ENGENEERING

ABCM Brazilian Society of Mechanical Sciences and Engineering
27th ABCM International Congress of Mechanical Engineering
December 04-08, 2023, Florianópolis-SC, Brazil

COB-2023-0467
PERFORMANCE VERIFICATION OF THE VOLUMETRIC THERMAL CAPACITOR METHOD APPLIED IN MOVING HEAT SOURCE AUTOGENOUS WELDING SIMULATION RUN IN GPU WITH ENHANCED PARALLELIZED CODE

Arthur Mendonça de Azevedo
Ernandes José Gonçalves do Nascimento
Elisan dos Santos Magalhães
Instituto Tecnológico de Aeronáutica – ITA, 12228-900, São José dos Campos – SP, Brasil
arthurama@ita.br
ernandes@ita.br
elisan@ita.br

Abstract. *The previous simulation of manufacturing processes allows the prediction of possible failures, the estimation of the final mechanical characteristics, and production cost reduction. The Computational Fluid Dynamics (CFD) techniques revolutionized modern product design by also requiring a lower number of experiments to achieve equal or better-quality results. The simulation outcomes provide several advantages such as easy variable probing at any point of the domain, operational risk reduction, elimination of experimental space and required apparatus, and a much faster solution. The computational time needed to produce reasonable numerical solutions has greatly dropped since the beginning of the CFD era. However, there is still plenty of room for large computing enhancements through better code and hardware coupling. To fulfill this gap, an example of the applicability of a parallelized CUDA-C language code is presented in this work. The authors verified the performance of The Volumetric Thermal Capacitor (VTC) method applied in the Laser Beam Welding (LBW) process simulation. Here, the algebraic form of the transient heat conduction Partial Differential Equation (PDE) was discretized by the Finite Volume Method (FVM) and computed in the Graphics Processing Unit (GPU) for a faster solution. The melting process was accounted for through the application of the enthalpy method employed with the VTC method. Here, a fixed grid approach allows for the prediction of a sharp phase change front through the calculation of the liquid fraction parameter. The heat loss due to radiation and convection effects as well as temperature-dependent properties were accounted for to increase the solution accuracy. The Successive Over-relaxation (SOR) solver was applied to obtain the final matrix governing equation solution. The applied hardware consisted of an RTX 3090 graphics card with 24 GB of video memory with double precision floating point operations capability. The research findings that the VTC method is an efficient model to analyze phase-change processes when it is compared with the classical model. Furthermore, it suggested that GPU processing offers reasonable reliability but also the great advantage of a much faster computational solution when compared to traditional serial computing.*

Keywords: *Volumetric Thermal Capacitor Method, GPU processing, CUDA-C language, Finite Volume Method, Autogenous welding.*

1. INTRODUCTION

Industrial manufacturing processes are among the most important modern economic activities. The previous simulation of the production methods is valuable for energy efficiency optimization, material waste reduction, and better dilution of the involved costs. In specific relation to welding techniques, Soltan and Omar (2022) recently discussed the essentiality of such methods to a large variety of applications in different industries, ranging from small products to very large projects. As a matter of fact, modern welding technologies are widely used in aerospace, automotive, shipping, petrochemical, and other industrial fields (Fan, Qin, Jiang, & Wang, 2023). As the welded materials are joined by a liquefication process followed by further solidification, the proper simulation of welding processes requires efficient mathematical modeling of the fusion, cooling, and solidification phenomena.

Following the evolution of the phase change modeling methods, the first investigations in this field were performed by Lamé and Clapeyron (1831) in a study regarding the earth's crust solidification. However, the first significative progress was with Stefan (1889), who analyzed the ice growth rate data published by British and German explorers, as described by Vuik (1993). Stefan (1889) was the first to propose that the square of the ice thickness in polar regions is a linear function of time. Hence, the moving boundary solidification problems would half a century later become widely known as the Stefan problem, in honor of its largest contributor. The nomenclature applied here denotes a particular kind of boundary value problem described by a system of Partial Differential Equations (PDEs) where the boundary between

the two phases moves with time. Later, Stefan finer adjusted the first model and defined a time-dependent temperature profile called *kältesumme*, or cold sum, as also presented in 1889. The cold sum model achieved a much better agreement with the experimental data. Crepeau (2008) highlights that after the developments of 1889 made by Stefan, the melting/solidification boundary problem became asleep until the mid-twentieth century.

Dacev (1947 and 1950) gave continuity to the study of Stefan phase change class of problems by publishing in Russian language notes regarding the linearity of such mathematical modeling. Crank (1957) then developed two methods to describe the numerical treatment of heat-flow problems in which a transforming boundary moves through the medium. In the first method, the problem was transformed from one involving a simple heat-conduction equation and a moving boundary to a fixed boundary eigenvalue problem. In the second method, Lagrangian interpolation formulae were used to develop finite-difference approximations to space derivatives of temperature based on values at points unequally spaced in the direction of heat flow. Later, Boley (1961) developed a method for heat conduction analysis for melting and solidification problems. The technique made use of a fictitious body with an unchanged shape identical to that of the body before any phase transformation. Hence, the original partial differential boundary value problem was now replaced by an ordinary integrodifferential one that can be solved numerically or in series form. Baceli and Melamed (1964) published a method for reducing the generalized Stefan problem to a limited boundary value problem. The developed technique made possible a simpler mathematical form for solving the melting-solidification phenomenon.

The research and developments on the Stefan problem continued in the works of Primicero (1970), Meyer (1971) and Rubinstein (1971). The first author developed generalizations based on the assumption that the latent heat is a given function of the position of the separation plane between the two phases. Meyer applied the method of lines to approximate the partial differential equations at discrete time levels in free interface problems to ordinary differential equations solved by conversion to initial value problems. Rubinstein performed a complete examination of the results concerning the classical Stefan problem (static materials and constant thermophysical properties) and its generalization with brief descriptions of proposed finite difference algorithms. Lastly, Voller et al. (1979) developed weak solution methods specifically aimed at solving Stefan's problems. Here the authors show that stable solutions may be obtained from enthalpy methods where phase change takes place over a temperature range. However, stability significantly decreases if the range becomes relatively small or degenerates to a single temperature.

Many phase change modeling advancements were made after the rise of numerical methods. Modern iterative solutions became an alternative to the traditional analytical approaches when attempting to accurately solve the Stefan problem. For instance, Voller and Cross (1981a) developed accurate solutions for moving boundary problems by applying the enthalpy method. At this point, the extension of the technique to two-dimensional problems was demonstrated by using a straightforward explicit method. The authors also described an implicit scheme for one-dimensional problems, which could simultaneously cope with any size melting temperature range and the influence of internal heating. Another work regarding the numerical solving of fusion and solidification phenomena was published by the authors in the same year (Voller and Cross, 1981a). Here, the researchers extended the one-dimensional algorithm previously developed to solve circular regions with spatially uniform boundary conditions. The study also contained a demonstration of how to numerically predict the solidification/melting phenomena at a circular cylinder using a single non-dimensional expression.

Continuing with the modern advancements in phase-change modeling, Voller and Prakash (1987) published a fixed grid numerical modeling methodology to solve convection-diffusion controlled mushy region phase change problems. The approach employed here was based on the representation of the latent heat and flow evolution in the solid-liquid mushy zone with suitable chosen sources. The method allowed for enough freedom within the methodology for the definition of such sources so that a variety of problems could be modeled. Brent et al. (1988) developed an enthalpy-porosity technique for modeling convection-diffusion phase change. The authors applied the method to numerically investigate the melting of pure gallium placed in a rectangular cavity. Here, the technique allowed for a fixed-grid solution of coupled momentum and energy equations to be undertaken without resorting to transformations in variables. The research results yielded excellent agreement between the numerical predictions and experimental results available in the literature. The two lastly cited works remain among the most scientifically relevant papers regarding numerical phase change modeling. Voller (1990a) then developed a rapid implicit solution technique for the enthalpy formulation of conduction-controlled phase change problems. The author first introduced three existing implicit enthalpy schemes with a new scheme later proposed and tested on a range of problems of one and two dimensions. A CPU performance comparison showed that the new scheme was between 1.5 and 10 times faster than the previous ones.

Voller et al. (1990b) published a review aimed at categorizing the major fixed grid formulations and solution methods for conduction-controlled phase change. The authors proposed a basic enthalpy equation for a two-phase solid-liquid model that received a few alternative formulations. The formulations were then reduced to a standard form in which the finite element and finite volume discretization were performed. The methods performed remained as the basis for a few phase-change fixed grid numerical solution techniques. Voller and Swaminathan (1991) developed a general source-based method to model solidification phase change. Here, the latent heat evolution was treated by a linearization of the discretized source term, yielding a robust and accurate computational method. The technique presented here may deal with several latent heat evolution mechanisms such as the modeling of a temperature-dependent liquid fraction.

More recently, Ren and Chan (2016) performed a GPU-accelerated numerical study of a Phase-Change Material (PCM) melting process in an enclosure with internal fins. The authors investigated the melting process in the PCM for

different materials of fins and walls, the number of fins, fin configurations, hot wall temperature, thermal boundary conditions, and inclination angle of the PCM cavity. The GPU methodology has proven to be an efficient approach for studying the fusion process. In previous work, Azevedo and Magalhães (2023) presented the Volumetric Thermal Capacitor (VTC) method for nonlinear heat transfer in phase-change materials. The technique was aimed at addressing the unsteady enthalpy term in the heat diffusion equation by applying the integration by parts rule to divide the enthalpy term into three components.

As seen in the previous literature review, the numerical methods became not only an alternative to analytical phase-change solutions but also made possible the modeling and solving of higher complexity melting and solidification phenomena such as three-dimensional simulations with natural and forced convection effects. However, there is still much room for enhancements in accuracy and computational efficiency in the field. Hence, the present research is aimed at demonstrating the application of a new phase change modeling methodology. The technique was applied here in treatment to the enthalpy term in the heat diffusion equation, thus resulting in better accuracy temperature fields during the materials' thermal cooling. The methodology was exemplified by executing an in-house parallelized CUDA-C language code to simulate a Laser Beam Welding (LBW) process. Here, an algebraic form of the transient heat conduction Partial Differential Equation (PDE) was discretized by the Finite Volume Method (FVM) and computed in a Graphics Processing Unit (GPU) for enhanced computational processing. The melting process was accounted for through a variation of the enthalpy method. Here, a fixed grid approach allows for the prediction of a sharp phase change front through the calculation of the liquid fraction parameter. The heat loss due to radiation and convection effects as well as temperature-dependent properties were accounted for to increase the solution accuracy. The Successive Over-relaxation (SOR) solver was applied to obtain the final matrix governing equation solution. The applied hardware consisted of an RTX 3090 graphics card with 24 GB of video memory with double precision floating point operations capability. The outcomings evidenced that the adopted phase change approach results in better temperature accuracy during the specimens' cooling. Finally, the research findings also suggested that GPU processing offers reasonable reliability but also the great advantage of a much faster computational solution when compared to traditional serial computing.

2. MATERIALS AND METHODS

2.1 The Laser Beam Welding (LBW) Problem

The LBW process simulated is schematized in Figure 1. The specimen has two thermocouples, 0 and 1, for measuring the temperature variation in the experiment. They are on the top surface of the specimen, the *xz*-plane. Likewise, the authors positioned five probe points, P_1 to P_5, transversely to the weld bead, also intended for temperature acquisition. These probe points are spaced 1.0 mm apart.

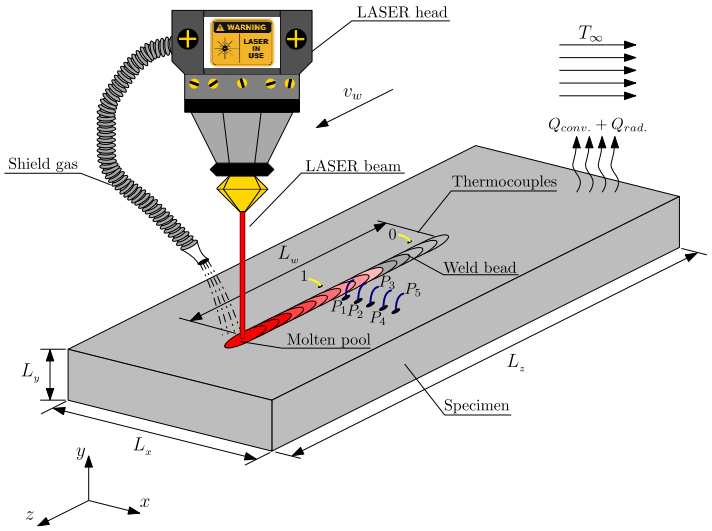

Figure 1. Laser Beam Welding (LBW) process schematics and parameters.

2.2 Mathematical Modeling

The applied heat conduction model is composed of the energy equation neglecting the advective effects and viscous dissipation. The mathematical modeling is given as,

$$\frac{\partial}{\partial x}\left(\lambda\frac{\partial T}{\partial x}\right)+\frac{\partial}{\partial y}\left(\lambda\frac{\partial T}{\partial y}\right)+\frac{\partial}{\partial z}\left(\lambda\frac{\partial T}{\partial z}\right)+q'''=\frac{\partial H}{\partial t} \tag{1}$$

where *x*, *y*, and *z* are the cartesian coordinates, *T* is the numerical temperature, λ is the non-linear thermal conductivity, q''' is the volumetric heat source and *t* is the time. The quantity *H* is the total enthalpy, which can be written as (Crank J. , 1984),

$$H=\underbrace{\int_{T_0}^{T}\rho(T)c(T)\,dT}_{\substack{\text{portion related to}\\ \text{the sensible heat}}}+\underbrace{\rho(T)\,f_L(T)\,L_f}_{\substack{\text{portion related to}\\ \text{the latent heat}}} \tag{2}$$

where ρ is the material density, *c* is the specific heat at constant pressure, f_L is the temperature-dependent liquid mass fraction function and L_f is the latent heat of fusion. In the case of isothermal phase change, *f*(T) is represented by the following,

$$f_L=f_L(T)=\begin{cases}0, \text{ if } T<T_m\\ 1, \text{ if } T>T_m\end{cases}$$
$$0<f_L=f_L(T)<1, \text{ if } T=T_m \tag{3}$$

where T_m is the material melting temperature.

The integral in Eq. (2) requires special treatment as presented in the VTC method (Azevedo & Magalhães, 2023). Then, applying the VTC mathematics steps, Eq. (1),

$$\frac{\partial}{\partial x}\left(\lambda\frac{\partial T}{\partial x}\right)+\frac{\partial}{\partial y}\left(\lambda\frac{\partial T}{\partial y}\right)+\frac{\partial}{\partial z}\left(\lambda\frac{\partial T}{\partial z}\right)+S=\rho c\frac{\partial T}{\partial t}+T\left(\rho\frac{\partial c}{\partial t}+c\frac{\partial \rho}{\partial t}\right)-\frac{\partial}{\partial t}\left[\int_0^T T\frac{\partial(\rho c)}{\partial T}dT\right]+L_f\left(\rho\frac{\partial f_L}{\partial t}+f_L\frac{\partial \rho}{\partial t}\right) \tag{4}$$

where *S* is the source term that brings together the contributions of internal energy generation and boundary conditions (heat flux, prescribed temperature, and insulation). Equation (4) presents a general formulation of the non-linear transient three-dimensional heat diffusion differential equation with the enthalpy function.

The specimen in Figure 1 was subjected to three different boundary conditions, in addition to the LBW heat source. The heat losses by natural convection and radiation were calculated based on Newton's law of cooling and the Stephan Boltzmann law, respectively. With these influences, the final heat loss equation may be written as,

$$-\lambda\frac{\partial T}{\partial \eta}=\underbrace{h(T)\left(T-T_\infty\right)}_{\substack{\text{Newton's law}\\ \text{of cooling}}}+\underbrace{\sigma\phi_{rad}(T)\left(T^4-T_\infty^4\right)}_{\text{Stephan Boltzmann law}} \tag{5}$$

where η is the direction normal to the surface, *h*(*T*) is the temperature-dependent heat transfer coefficient, σ is the Stefan Boltzmann constant, and ϕ_{rad} is the material's emissivity. Furthermore, forced convection modelled the shield gas influence, with a Single Round Nozzle model (Martin, 1977). In this case, this boundary condition is the same as presented by Azevedo and Magalhães (2023).

2.3 Moving Heat Source

The moving heat source was modeled as a Gaussian whole conical volumetric profile, as defined, and reviewed in previous works (Nascimento, Magalhães, & dos Santos Paes, 2023; Magalhães, et al., 2018). The mathematical modeling of the heat distribution is given as,

$$S=\frac{\dot{Q}}{0.460251h_p r_w^2}e^{-\frac{4.5\left(z-v_w t\right)^2}{r_w^2}}e^{-\frac{4.5\left(z-L_x/2\right)^2}{r_w^2}}\left(1-\frac{y^{1/2}}{h_p^{1/2}}\right) \tag{6}$$

where $\dot{Q}$ is the laser heat source power, h_p is the height of penetration, r_w is the welding radius and v_w is the welding head velocity.

2.4 Numerical solution

Integrating Eq. (4) into the time interval t to $t+\Delta t$ and applying the Finite Volume Method (FVM),

$$2\lambda_e \frac{T_E^{i+1}-T_P^{i+1}}{\Delta x_P(\Delta x_P+\Delta x_E)} - 2\lambda_w \frac{T_P^{i+1}-T_W^{i+1}}{\Delta x_P(\Delta x_P+\Delta x_W)} + 2\lambda_n \frac{T_N^{i+1}-T_P^{i+1}}{\Delta y_P(\Delta y_P+\Delta y_N)} - 2\lambda_s \frac{T_P^{i+1}-T_S^{i+1}}{\Delta y_P(\Delta y_P+\Delta y_S)} + 2\lambda_f \frac{T_F^{i+1}-T_P^{i+1}}{\Delta z_P(\Delta z_P+\Delta z_F)}$$
$$-2\lambda_b \frac{T_P^{i+1}-T_B^{i+1}}{\Delta z_P(\Delta z_P+\Delta z_B)} + S = \frac{\rho_P^{i+1}c_P^{i+1}(T_P^{i+1}-T_P^i)}{\Delta t} + \frac{T_P^{i+1}\left[\rho_P^{i+1}\left(c_P^{i+1}-c_P^i\right)+c_P^{i+1}\left(\rho_P^{i+1}-\rho_P^i\right)\right]}{\Delta t} - \frac{G_P^{i+1}-G_P^i}{\Delta t} \tag{7}$$
$$+\frac{\rho_P^{i+1}L(f_P^{i+1}-f_P^i)}{\Delta t} + \frac{f_P^{i+1}L(\rho_P^{i+1}-\rho_P^i)}{\Delta t}$$

where the subscripts *P*, *E*, *W*, *N*, *S*, *F*, *B* is the center of the polyhedron CV, east, west, north, south, front and back CV neighbors, respectively; the subscripts *e*, *w*, *n*, *s*, *f*, *b* is the east, west, north, south, front and back boundaries between CV, respectively; the superscript *i* is the time step counter; G_P^i and G_P^{i+1} is defined as,

$$G_P^{i+1} = \int_0^{T_P^{i+1}} T\frac{\partial(\rho c)}{\partial T}dT \quad \text{and} \quad G_P^i = \int_0^{T_P^i} T\frac{\partial(\rho c)}{\partial T}dT \tag{8}$$

Considering the harmonic mean to calculate the thermal conductivities of the CV boundaries,

$$\lambda_e = \frac{\lambda_P\lambda_E(\Delta x_P+\Delta x_E)}{\lambda_E\Delta x_P+\lambda_P\Delta x_E}, \quad \lambda_w = \frac{\lambda_P\lambda_W(\Delta x_P+\Delta x_W)}{\lambda_W\Delta x_P+\lambda_P\Delta x_W}, \quad \lambda_n = \frac{\lambda_P\lambda_N(\Delta y_P+\Delta y_N)}{\lambda_N\Delta y_P+\lambda_P\Delta y_N}$$
$$\lambda_s = \frac{\lambda_P\lambda_S(\Delta y_P+\Delta y_S)}{\lambda_S\Delta y_P+\lambda_P\Delta y_S}, \quad \lambda_f = \frac{\lambda_P\lambda_F(\Delta z_P+\Delta z_F)}{\lambda_S\Delta z_F+\lambda_P\Delta z_F}, \quad \lambda_b = \frac{\lambda_P\lambda_B(\Delta z_P+\Delta z_B)}{\lambda_B\Delta z_P+\lambda_P\Delta z_B} \tag{9}$$

Substituting Eq. (9) in Eq. (7) and rearranging the common terms, the VTC numerical model can be written as,

$$a_P T_P^{i+1} = a_E T_E^{i+1} + a_W T_W^{i+1} + a_N T_N^{i+1} + a_S T_S^{i+1} + a_F T_F^{i+1} + a_B T_B^{i+1} + b \tag{10}$$

where,

$$a_E = \frac{2\lambda_E\lambda_P}{\Delta x_P(\lambda_E\Delta x_P+\lambda_P\Delta x_E)}, \quad a_W = \frac{2\lambda_W\lambda_P}{\Delta x_P(\lambda_W\Delta x_P+\lambda_P\Delta x_W)}, \quad a_N = \frac{2\lambda_N\lambda_P}{\Delta y_P(\lambda_N\Delta y_P+\lambda_P\Delta y_N)}$$
$$a_S = \frac{2\lambda_S\lambda_P}{\Delta y_P(\lambda_S\Delta y_P+\lambda_P\Delta y_S)}, \quad a_F = \frac{2\lambda_F\lambda_P}{\Delta z_P(\lambda_Z\Delta z_P+\lambda_P\Delta z_F)}, \quad a_B = \frac{2\lambda_B\lambda_P}{\Delta z_P(\lambda_B\Delta z_P+\lambda_P\Delta z_B)} \tag{11}$$

$$a_P = a_E + a_W + a_N + a_S + a_F + a_B + \frac{\rho_P^{i+1}c_P^{i+1} + \rho_P^{i+1}\left(c_P^{i+1}-c_P^i\right)+c_P^{i+1}\left(\rho_P^{i+1}-\rho_P^i\right)}{\Delta t}, \tag{12}$$

$$b = S + \frac{\rho_P^{i+1}c_P^{i+1}}{\Delta t}T_P^i + \frac{(G_P^{i+1}-G_P^i)}{\Delta t} - \frac{\rho_P^{i+1}L(f_P^{i+1}-f_P^i)}{\Delta t} - \frac{f_P^{i+1}L(\rho_P^{i+1}-\rho_P^i)}{\Delta t} \tag{13}$$

where *a* is the coefficients and *b* is the total source term.

2.5 Geometry, Grid and Simulation Parameters

The variables illustrated in Figure 1 as well as the other applied simulation parameters are presented in Table 1.

Table 1. Simulation parameters.

Parameter	Values
Specimen length at *x*, *y* and *z*-directions, L_x, L_y, and L_z [mm]	30.0, 9.5, 70.0
Weld bead length, L_w [mm]	45.0
Specimen initial temperature [°C]	22.0
Room temperature, T_∞ [°C]	22.0
Laser head velocity, v_w [mm/min]	3000.0
Time-step, Δt [s]	1×10^{-3}
Simulation total time [s]	5.0
Welding radius, r_w [mm]	0.5
Height of penetration, h_p [mm]	1.91
Laser power, $\dot{Q}$ [W]	2400.0
Shield gas	Argon
Gas Prandtl number	Range: 0.668 to 0.669
Gas thermal conductivity	Range: 0.012 to 0.089
Gas Kinematic viscosity	Range: 6.55×10^{-6} to 7.06×10^{-4}
Gas flow [L/min]	15
Diameter of round nozzle [mm]	10
Distance between nozzle exit and solid surface [mm]	300
Gas temperature [°C]	-0.94

2.6 Material Properties

The authors used the SAE 1020 steel as the sample material for the experimental setup exposed in Figure 1. Table 2 presents the material thermal properties considered in this paper.

Table 2. SAE 1020 steel thermal properties.

Thermal properties (SAE 1020)	Values / Equations
ρ [kg/m³]	7,780.0
λ [W/m.K]	$\lambda(T) = 2.5\times10^{-5}T^2 - 0.053T + 57.2$
c [J/kg.K]	$c(T) = 2.785\times10^2 e^{1.196\times10^{-3}T}$
ϕ_{rad}	$\phi_{rad}(T) = 8.47\times10^{-2}\ln(T) - 39.32\times10^{-2}$
L_f [kJ/kg]	247.0
Melting Temperature, T_m	1450.0

3. RESULTS AND DISCUSSION

In this section, the authors compared the results between the VTC method, and the classical model (de Azevedo, Magalhães, da Silva, & Lima e Silva, 2022) applied in the LBW simulation. These models were compared with the LBW experiment shown by Magalhães (2018).

3.1 Grid convergence test

A grid size independence study was performed for the higher variation temperature experiment. The authors assumed five different nonuniform grid sizes for the LBW experiment. The size of tested grids ranged from 388,080 to 2,906,112 Control Volume (CV). Table 3 presents all tests performed for thermocouple 1, according to their position in Figure 1. In agreement with Table 3, a grid size independence study resulted in a choice of nonuniform grid with 1,750,100 CV.

Table 3. Grid size independence.

Grid size [CV]	Temperature variation concerning the grid with 2,906,112 CV [%]	Numerical solution time
388,080	4.14	1 min 44 s
888,300	1.43	3 min 41 s
1,308,354	1.22	5 min 7 s
1,750,100	0.51	6 min 37 s
2,906,112	-	11 min 12 s

3.2 Sensitivity analysis

Applying the sensitivity analysis is a good way to verify the performance of a model given an input parameter oscillation. The sensitivity coefficient for a single sensor is defined as (Magalhães, 2021),

$$S = X_i \frac{\partial T}{\partial X_i} \tag{14}$$

Considering the numerical derivative, Eq. (14) can be written as,

$$S = X_i \frac{T(X_i) - T(X_i + \delta)}{\delta} \tag{15}$$

where,

$$\delta = X_i \times 10^{-3} \tag{16}$$

This work considered an oscillation in the LBW heat flux to compare the VTC and classical model concerning time steps. Figure 2 presents the sensitivity coefficient for these two models at Thermocouple 1. In this case, it is possible to note more sensitivity in the phase-change process in both models. However, the VTC model is more sensitivity than the classical model in the cooling process.

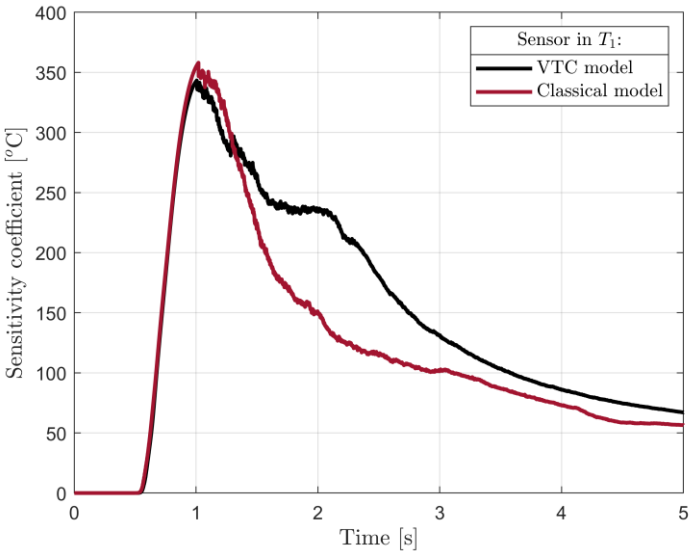

Figure 2. Sensitivity coefficient in the Thermocouple 1.

3.3 Comparison between VTC and classical models

The LBW experimental verification considered the thermocouple 0 and 1, according to their positions in Figure 1. Furthermore, the numerical simulation considered the probe points P_1 to P_5 (Figure 1) to verify the performance of the VTC and classical models. Figure 3 presents the experimental results and the numerical solution with these models. In

the LBW experiment, the heating and cooling rates are rapid and intense. The classical model did not show good agreement with the experimental results, unlike the proposed model. The most significant residue, for both thermocouples 0 and 1, was 6% and it was registered during the cooling process. Figure 4a shows numerical simulation results for the probe points P_1 to P_5 for the VTC and classical models. As expected, the heating and cooling rates directly influence the differences between the models. The closer to the LBW heat flux, the higher the heating rates. Consequently, the higher the percentage change rate, as shown in Figure 4b. This behavior was the same that Azevedo and Magalhães (2023) presented with the simulated experiments, demonstrating the validity of the theory for the cases with intense and rapid heating and cooling.

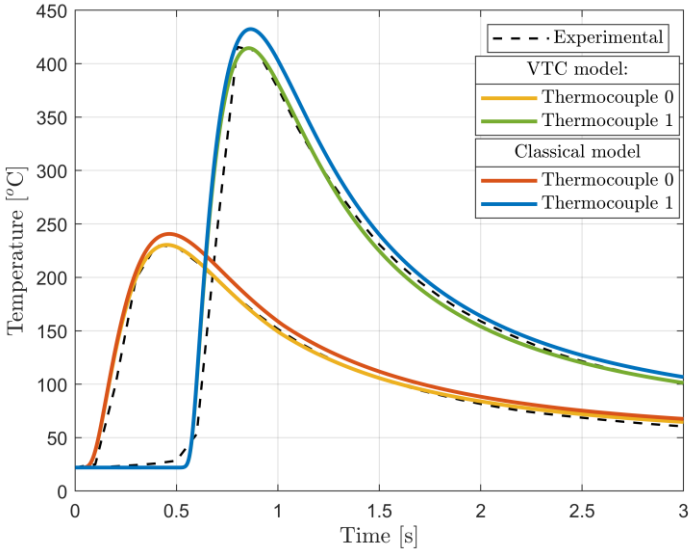

Figure 3. The LBW experiment and the numerical solutions for the two models.

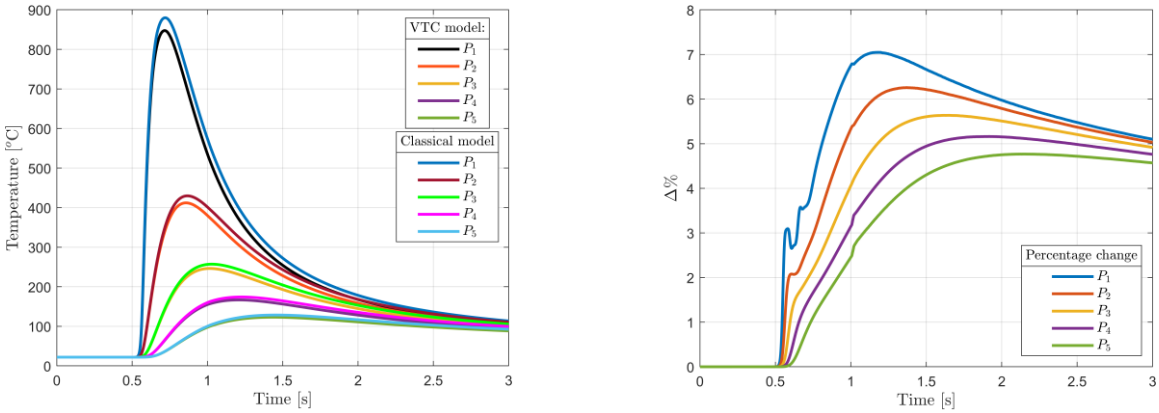

(a) Numerical simulation. (b) Comparison between the models.

Figure 4. Probe points P_1 to P_5 results for the VTC and classical models.

4. CONCLUSION

The authors showed the VTC methodology which applies the enthalpy method in heat conduction simulation. For this, the VTC model is based on non-linear thermal properties without simplifications or generalized considerations.

The following conclusions were achieved so far in the development of the present research:

- With the grid size independence study was possible to verify an excellent performance in GPU processing, that offers great computational time advantage when compared to traditional serial computing.
- The sensitivity analysis, with the oscillation in the LBW heat flux, proved that the VTC model has better adjustment in the cooling process when compared to the classical model.

- For the performance verification of the VTC and classical models, this work presented the numerical simulation of the LBW experiment. If the heating and cooling rates are rapid and intense, the percentage change between these models is more significant. The achieved results proved that VTC is an efficient model to analyze phase-change processes.

5. ACKNOWLEDGEMENTS

The authors would like to thank CAPES (an agency of the Ministry of Education of Brazil), CNPq (an agency of the Ministry of Science, Technology, Innovations, and Communications of Brazil), and PETROBRAS (a Brazilian multinational company) for the invaluable financial support.

6. REFERENCES

Azevedo, A., & Magalhães, E. (2023). The volumetric thermal capacitor method for nonlinear heat transfer in phase-change materials. *International Communications in Heat and Mass Transfer*, 106672.

Bergman, S. (1952). The solution of boundary value problems by the method of the kernel function. *Proceedings of the 1952 ACM national meeting* (pp. 187 - 192). Pittsburgh: ACM.

Boley, B. (1961). A Method of Heat Conduction Analysis of Melting and Solidification Problems. *Journal of Mathematics and Physics*, 300 - 313.

Brent, A., Voller, V., & Reid, K. (1988). Enthalpy-porosity technique for modeling convection-diffusion phase change: application to the melting of a pure metal. *Numerical Heat Transfer*, 297 - 318.

Crank, I. (1957). Two methods for the numerical solution of moving-boundary problems in diffusion and heat flow. *The Quarterly Journal of Mechanics and Applied Mathematics*, 220 - 231.

Crank, J. (1984). *Free and Moving Boundary Problems.* Oxford, UK: Oxford University Press.

Crepeau, J. (2008). Josef Stefan and His Contributions to Heat Transfer. *2008 Proceedings of the ASME Summer Heat Transfer Conference, HT 2008.* ASME.

Dacev, A. (1950). On the linear problem of Stefan. The case of two phases of infinite plates. *Dokl. Akad. Nau k SSS R*, 445 - 448.

Dacev, A. B. (1947). On the linear problem of Stefan. *Dokl. Akad. Nau k SSS R*, 563 - 566.

de Azevedo, A. M., Magalhães, E. d., da Silva, R. D., & Lima e Silva, S. M. (2022). A comparison between nonlinear and constant thermal properties approaches to estimate the temperature in LASER welding simulation. *Case Studies in Thermal Engineering*, p. 102135.

Fan, X., Qin, G., Jiang, Z., & Wang, H. (2023). Comparative analysis between the laser beam welding and low current pulsed GMA assisted high-power laser welding by numerical simulation. *Journal of Materials Research and Technology*, 2549 - 2565.

Lamé, G., & Clapeyron, E. (1831). Mémoire sur la solidification par refroidissement d'un globe liquide. *Annales de Chimie et de Physique*, 250 - 256.

Magalhães, E. S. (Dec de 2021). A quadrilateral optimization method for non-linear thermal properties determination in materials at high temperatures. *International Journal at Heat and Mass Transfer*, p. 121857.

Magalhães, E. S., Paes, L. d., Pereira, M., da Silveira, C. A., Pereira, A. d., & Lima e Silva, S. M. (March de 2018). A thermal analysis in laser welding using inverse problems. *International Communications in Heat and Mass Transfer*, pp. 112-119.

Magalhães, E., dos Santos Paes, L., Pereira, M., da Silveira, C., de Souza Pinto Pereira, A., & Lima e Silva, S. (2018). A thermal analysis in laser welding using inverse problems. *International Communications in Heat and Mass Transfer*, 112 - 119.

Martin, H. (1977). Heat and Mass Transfer between Impinging Gas Jets and Solid Surfaces. pp. 1-60.

Meyer, G. (1971). A Numerical Method for Two-Phase Stefan Problems. *SIAM Journal on Numerical Analysis*, 555 - 568.

Nascimento, E., Magalhães, E., & dos Santos Paes, L. (2023). A literature review in heat source thermal modeling applied to welding and similar processes. *The International Journal of Advanced Manufacturing Technology*, 2917 - 2957.

Primicero, M. (1970). Stefan- like problems with space- dependent latent heat. *Meccanica*, 187 - 190.

Ren, Q., & Chan, C. (2016). GPU accelerated numerical study of PCM melting process in an enclosure with internal fins using lattice Boltzmann method. *International Journal of Heat and Mass Transfer*, 522 - 535.

Rubinstein, L. I. (1971). The Stefan Problem. *American Mathematical Society*, 356 - 419.

Soltan, H., & Omar, M. (2022). A roadmap for selection of metal welding process: a review and proposals. *Welding in the World*, 2639 - 2675.

Stefan, J. (1889). "Über die Theorie der Eisbildung insbesondere über die Eisbildung im Polarmeere. *Sitzungsberichte der kaiserlichen Akademie der*, 965 - 983.

Voller, V. R. (1990a). Fast implicit finite-difference method for the analysis of phase change problems. *Numerical Heat Transfer, Part B: Fundamentals*, 155 - 169.
Voller, V. R., Cross, M., & Walton, P. (1979). Assessment of weak solution techniques for solving Stefan problems. p. 172.
Voller, V., & Cross, M. (1981a). Accurate solutions of moving boundary problems using the enthalpy method. *International Journal of Heat and Mass Transfer*, 545 - 556.
Voller, V., & Cross, M. (1981b). Estimating the solidification/melting times of cylindrically symmetric regions. *International Journal of Heat and Mass Transfer*, 1457 - 1462.
Voller, V., & Prakash, C. (1987). A fixed grid numerical modelling methodology for convection-diffusion mushy region phase-change problems. *International Journal of Heat and Mass Transfer*, pp. 1709 - 1719.
Voller, V., & Swaminathan, C. (1991). General source-based method for solidification phase change. *Numerical Heat Transfer, Part B: Fundamentals*, 175 - 189.
Voller, V., Swaminathan , C., & Thomas, B. (1990b). Fixed grid techniques for phase change problems. A review. *International Journal for Numerical Methods in Engineering*, 875 - 898.
Vuik, C. (1993). Some historical notes on the Stefan problem. *Nieuw Archief voor Wiskunde*, 157 - 167.

7. RESPONSIBILITY NOTICE

The authors are the only responsible for the printed material included in this paper.